RSC Advances

PAPER

View Article Online
View Journal | View Issue

Cite this: *RSC Adv.*, 2021, **11**, 39233

Theoretical and experimental studies on uranium(VI) adsorption using phosphine oxide-coated magnetic nanoadsorbent

Zeinab F. Akl

In this study, novel Cyanex-923-coated magnetite nanoparticles (Fe_3O_4@Cyanex-923) were prepared, comprehensively characterized, and employed for uranium(VI) ion adsorption from aqueous solutions. FTIR and TGA data confirmed that Fe_3O_4 has successfully gained Cyanex-923 surface functionality. Particle size and morphological studies *via* DLS, HR-TEM, and SEM showed uniform-dispersed quasi-spherical nanoparticles with a mean diameter of *ca.* 44 nm. Magnetism measurement data revealed the superparamagnetic properties of the Fe_3O_4@Cyanex-923 nanoadsorbent. The effect of different experimental settings on the adsorption efficiency was studied to determine the best operational conditions. The experimental results were analyzed using Langmuir, Freundlich, and Temkin isotherms; where the adsorption data obeyed the Langmuir model showing a theoretical adsorption capacity of 429.185 mg g^{-1} at 298 K. Kinetics data analysis revealed a fast adsorption process that could reach equilibrium within 60 min and is well-fitted to the pseudo-2nd-order model. Temperature affected the adsorption process and the thermodynamic data indicated that uranium(VI) adsorption was spontaneous and exothermic. Fe_3O_4@Cyanex-923 nanoparticles displayed a good regeneration behavior over three sequential adsorption–desorption cycles. The Fe_3O_4@Cyanex-923 nanoadsorbent showed a high uranium adsorption capacity, fast equilibration time, economic nature, good reusability, and easy separation; making it a promising candidate for uranium(VI) removal from nuclear waste streams.

Received 10th June 2021
Accepted 30th November 2021

DOI: 10.1039/d1ra04515f

rsc.li/rsc-advances

1. Introduction

The magnetic separation technique is one of the most recognized and widely used methods for water and wastewater treatment.[1] The process involves contaminant attachment onto a magnetic material's surface followed by separation of the contaminant-laden material *via* an externally employed magnetic force.[2] Magnetic adsorbents have continuously received growing attention due to their numerous advantages including fabrication simplicity, cost-adequateness, high adsorption capacities, rapidness, and convenience.[2] Their facile and economic separation from the aqueous solutions *via* applying a magnetic field makes them feasible materials for efficient and sustainable adsorption processes.[3] Thus, the utilization of magnetic adsorbents can lead to a simple, environmentally-friendly, time-saving, and cost-effective adsorption process as it evades the filtration and centrifugation steps while the magnetic adsorbent can be easily collected and reused.[4]

Among magnetic iron oxides, magnetite (Fe_3O_4) is widely investigated for the environmental remediation as well as other numerous applications including biomedicine, sensors, catalysis, energy storage devices, and magnetic resonance imaging.[5] Owing to their inexpensive production strategy, availability, physiochemical properties, nontoxic character, ease of modification, biocompatibility, ecological suitability, stability, superparamagnetism, recoverability, and recyclability; Fe_3O_4-based adsorbents have a considerable potential for removing a wide range of organic and inorganic contaminants from water streams.[6] The nanoscale dimension of Fe_3O_4 can be developed leading to an enhanced performance under various environmental circumstances.[7] The high surface area of Fe_3O_4 nanoparticles along with their susceptibility to the magnetic fields; have made them attractive materials for efficient removal of water impurities.[4]

Uranium is the most common naturally occurring radionuclide that possesses different forms and oxidation states.[8] Excessive uranium quantities are discharged to the environment from many anthropogenic activities *e.g.*, mining, milling, spent fuel reprocessing, improper nuclear waste management, nuclear testing, nuclear accidents, and phosphate fertilizers industry.[8] Such activities increase the potential of uranium contamination in natural waters (ground and surface water) that may be adsorbed and concentrated by plants and consequently reach the food chain.[8] Accordingly, uranium would hand over to humans and could finally accumulate in various organs to cause acute or chronic health problems; such as

Egyptian Atomic Energy Authority, P.O. Box 11762, Cairo, Egypt. E-mail: eltasneem2007@yahoo.com

tubular necrosis, skin corrosion, leukemia, bone cancer, kidney failure, liver or brain damage, and even death.[9] As a result, uranium removal from water streams has become one of the main environmental remediation issues nowadays.

Various technologies have been applied to remove uranium from contaminated water, nevertheless; adsorption is considered an effective method that has gained wide interest among the nuclear industry scientists. Over the last decades, developing efficient uranium adsorbents has been a research focus. Numerous organic and inorganic materials have been developed and assessed for their affinity towards uranium such as amidoxime-based,[10] carbon-based,[11] biochar-based,[12,13] metal organic frameworks-based,[14] covalent organic frameworks-based composites[15,16] and nanocomposites.[17] Among them, nanometric scale adsorbents are of particular concern due to their inimitable properties, as they have high specific surface area, elevated reactivity, high adsorption efficiency and capacity, fast adsorption rate, and acceptable reusability. In this context, diverse nanomaterials have been developed to remove uranium from aqueous media, including carbon nanotubes,[18] graphene nanocomposites,[19] nanoscale zero-valent iron,[20] and functionalized Fe_3O_4 nanoparticles.[21]

During the last decades, bare and coated Fe_3O_4 nanoparticles have been widely investigated for uranium entrapment.[22–25] Utilization of Fe_3O_4 nanoparticles for uranium remediation conforms to the environmental and human safety considerations; as they can be easily and remotely controlled and separated and consequently reduces the radiation exposure.[6] Fe_3O_4 nanoparticles can be readily coated with a variety of functional groups, where their affinity towards uranium can be enhanced by their surface modification with materials having a good binding capability for uranium.[24] Up to now, several studies have investigated the removal of uranium by Fe_3O_4 nanoparticles coated with various organic and inorganic materials.[22–28]

Organophosphorus compounds have good affinity and selectivity for actinides and were extensively tested for uranium extraction from nuclear waste streams.[29,30] In particular, trialkylphosphine oxides are cost-effective neutral extractant with demonstrated high extraction capacity and high stability in strong acidic media, which makes them are excellent ligands to functionalize various adsorbents for uranium capture.[31,32] Cyanex-923 is a promising phosphine oxide extractant which revealed high radiation stability, good hydrolysis resistance, poor water solubility, and non-corrosive nature;[33,34] thus, it could be a potential candidate to be impregnated onto the Fe_3O_4 surface for the efficient uranium adsorption.

Although coating of Fe_3O_4 nanoparticles is a well-established method to enhance their adsorption efficiency, there is no work carried out on coating the surface of Fe_3O_4 nanoparticles by Cyanex-923, to the author's knowledge. While plentiful studies have been reported on uranium(VI) adsorption *via* various adsorbents, the feasibility of uranium(VI) adsorption on Fe_3O_4@Cyanex-923 nanoadsorbent has not been tested yet. Thus, motivated by combining the features of simple magnetic separation and efficient uranium extraction; this work reports Cyanex-923 utilization for coating the Fe_3O_4 nanoparticles in order to design a novel uranium(VI) nanoadsorbent. Uranium remediation from water systems was investigated in relation to the medium acidity, Fe_3O_4@Cyanex-923 dose, initial concentration, and temperature. Besides, the adsorption isotherms, kinetics, and thermodynamics studies were conducted.

2. Experimental

2.1. Reagents

The reagents used throughout the experimental work were of analytical grade. Ferrous chloride, ferric chloride, and arsenazo-III were obtained from Sigma-Aldrich (Saint Louis, USA). Nitric acid, sodium hydroxide, ammonia solution, sodium carbonate, oleic acid, and ethanol were obtained from Merck (Darmstadt, Germany). Cyanex-923 was provided by Solvay/Cytec (Ontario, Canada). Uranium nitrate hexahydrate was used to prepare the working uranium(VI) solutions.

2.2. Fe_3O_4@Cyanex-923 preparation

Fe_3O_4 nanoparticles were first prepared according to the literature[35] by mixing acidified ferric and ferrous chloride solutions in a 2 : 1 molar ratio, under vigorous stirring and nitrogen purging. Then, the pH was increased to 9 and the reaction was kept at 80 °C for 60 min using oleic acid as dispersant.[35] The produced Fe_3O_4 nanoparticles were separated by a magnet and washed with excessive ethanol.

Cyanex-923 coated Fe_3O_4 nanoparticles were obtained by dispersing a known weight of the prepared Fe_3O_4 nanoparticles in Cyanex-923 ethanolic solution (0.150 mol L^{-1}, 50 mL) followed by overnight shaking at room temperature. Then, the product was collected using an external magnet, washed with ethanol, and vacuum-dried to a fixed weight.

2.3. Fe_3O_4@Cyanex-923 characterization techniques

Fourier transmission infrared spectroscopy (FTIR, Nicolet iS10 FTIR spectrophotometer, Thermo Scientific, Japan) was used for detecting the functional groups of Fe_3O_4@Cyanex-923. Dynamic light scattering (DLS) analysis was utilized to determine the particles diameter of Fe_3O_4@Cyanex-923 using PSS-NICOMP particle sizer (380ZLS, 40 mW, nominal wavelength 632.8 nm, PSS-NICOMP, Santa Barbara, CA, USA). The morphology of Fe_3O_4@Cyanex-923 was investigated by a high-resolution transmission electron microscope (HR-TEM, JEM 2100, JEOL, Japan) and scanning electron microscope (SEM, 6510 LA, JEOL, Japan). A thermogravimetric analyzer (TGA, Shimadzu TGA-50, Japan) was used to investigate the thermal stability of Fe_3O_4@Cyanex-923 within the temperature range 25–750 °C, at heating and nitrogen flow rates of 10 °C min^{-1} and 20 mL min^{-1}, respectively.

2.4. Fe_3O_4@Cyanex-923 adsorption performance

In a typical batch experiment, 30 mg of Fe_3O_4@Cyanex-923 was placed in a conical flask containing uranium(VI) solution adjusted at pH 5 by a calibrated combination glass electrode (Sentek, UK). After shaking at 25 °C for 60 min, Fe_3O_4@Cyanex-923 was magnetically separated and the residual uranium

concentration was measured by a UV-Visible spectrophotometer (Thermo evolution 300, UK).

The adsorption efficiency of uranium(VI) on Fe_3O_4@Cyanex-923 (E_A%) was determined from the difference of the starting and equilibrium uranium(VI) concentrations according to the following equation:

$$E_A\% = \frac{(C_o - C_e)}{C_o} \times 100 \quad (1)$$

where, C_o and C_e represent uranium starting and equilibrium concentrations (mg L^{-1}), respectively.

The uranium(VI) quantity adsorbed through Fe_3O_4@Cyanex-923 unit weight (q_e, mg g^{-1}) was determined from the subsequent expression:[26]

$$q_e = \frac{(C_o - C_e) \times V}{W} \quad (2)$$

where, V represents the solution volume (L) and W represents Fe_3O_4@Cyanex-923 weight (g).

To evaluate the pH effect on uranium adsorption, the adsorption experiments were carried out while varying the solution pH from 2 to 9. Briefly, aliquots of pH-adjusted uranium(VI) solutions with identical concentrations were added to a constant weight of Fe_3O_4@Cyanex-923 and stirred at 25 °C for a fixed time. Finally, the uranium content remaining in the solution was spectrophotometrically measured.

The adsorption behavior of bare Fe_3O_4 nanoparticles towards uranium(VI) was also investigated under the same conditions.

2.5. Adsorption kinetics

To investigate the contact time effect on uranium(VI) adsorption, the adsorbent (30 mg) was shaken with a series of uranium(VI) solutions of identical concentration and pH for different time intervals (0–200 min), then the uranium content in each solution was analyzed after separating the nanoadsorbent magnetically.

The experimental results were treated by the pseudo-1st-order and pseudo-2nd-order kinetics models given by the following formulas, respectively:[17]

$$\log(q_e - q_t) = \log q_e - \frac{k_1}{2.303} t \quad (3)$$

$$\frac{t}{q_t} = \frac{1}{k_2 q_e^2} + \frac{1}{q_e} t \quad (4)$$

where q_e and q_t represent uranium(VI) quantities (mg g^{-1}) adsorbed at equilibrium and time t (min), respectively. While k_1 and k_2 are the pseudo-1st-order (min^{-1}) and pseudo-2nd-order (g mg^{-1} min^{-1}) rate constants, respectively.

The chi-square test (χ^2) was further used to validate the kinetic models fitting to the experimental data and was determined as follows:[36]

$$\chi^2 = \sum \frac{(q_{exp} - q_{cal})^2}{q_{cal}} \quad (5)$$

where q_{exp} and q_{cal} are quantities of adsorbed uranium(VI) at equilibrium (mg g^{-1}), experimentally determined and theoretically computed, respectively.

Moreover, the pseudo-2nd-order fitting data was used to compute the initial adsorption rate (h, mg g^{-1} min^{-1}) as follows:[35]

$$h = k_2 q_e^2 \quad (6)$$

2.6. Adsorption isotherms

Isotherms investigations were conducted by equilibrating the magnetic nanoadsorbent with uranium(VI) solutions of different concentrations (25–200 mg L^{-1}) while maintaining the experimental settings fixed and then treated as previously described.

The experimental results were analyzed by three adsorption isotherm models; namely Langmuir, Freundlich, and Temkin. The Langmuir isotherm model is expressed as:[27]

$$\frac{C_e}{q_e} = \frac{C_e}{q_{max}} + \frac{1}{q_{max} K_L} \quad (7)$$

where C_e and q_e are as described earlier, q_{max} (mg g^{-1}) represents the maximal single-layer coverage capacity, and K_L is Langmuir parameter (L mg^{-1}). The linear plot of C_e/q_e *vs.* C_e has intercept and slope values equal to $1/q_{max}K_L$ and $1/q_{max}$, respectively.

The essential characteristics of Langmuir model are described through a non-dimensional parameter known as separation factor (R_L) that explains the favorability of the adsorption process and can be calculated from the subsequent formula:[36]

$$R_L = \frac{1}{1 + K_L C_o} \quad (8)$$

Freundlich isotherm model is given by the following equation:[28]

$$\log q_e = \log k_F + \frac{1}{n} \log C_e \quad (9)$$

where, K_F is Freundlich constant (mg g^{-1}) and n is an empirical parameter indicating the adsorption favorability (L g^{-1}), and their values are obtainable from plotting $\log q_e$ *vs.* $\log C_e$.

Temkin isotherm model is expressed as:[37]

$$q_e = B \ln A_T + B \ln C_e \quad (10)$$

where, B is constant related to the adsorption heat (J mol^{-1}) and is expressed as $B = \frac{RT}{b_T}$, b_T is Temkin constant, T is the absolute temperature (K), R is the gas constant (8.314 J mol^{-1} K^{-1}), and A_T is Temkin equilibrium binding constant (L g^{-1}). Temkin constants can be calculated from plotting q_e *vs.* $\ln C_e$.

2.7. Adsorption thermodynamics

The variation of energy during the adsorption process was investigated through calculating the thermodynamic parameters. The linear regression plotting of $\ln K_c$ *vs.* $1/T$ according to eqn (11) enables the calculation of enthalpy (ΔH°) and entropy

(ΔS°) from the plot slope and the intercept, respectively. The Gibbs free energy (ΔG°) can be calculated using eqn (12):[28,36]

$$\ln K_c = \frac{\Delta S^\circ}{R} - \frac{\Delta H^\circ}{RT} \quad (11)$$

$$\Delta G^\circ = RT \ln K_c \quad (12)$$

where, R is the gas constant (8.314 J mol^{-1} K^{-1}), T is the absolute temperature (K), and K_c is the adsorption equilibrium constant expressed as $K_c = \frac{q_e}{C_e}$.

2.8. Regeneration and reusability studies

Regeneration experiments were performed in batch mode for three consecutive cycles. Initially, the magnetic nanoadsorbent was added to uranium solution of 50 mg L^{-1} adjusted at pH 5 and then the solution was agitated at room temperature. When the adsorption equilibrium was attained the magnetic nanoadsorbent was magnetically isolated, washed with deionized water to remove the unbounded uranium, and dried to a fixed weight. Then, this nanoadsorbent was treated with various desorption agents (0.5 mol L^{-1} Na_2CO_3 and 0.01 mol L^{-1} HNO_3) at room temperature for 120 min under shaking conditions. Afterward, the concentration of uranium released into the solution was determined spectrophotometrically. To assess the reusability of the magnetic nanoadsorbent, the described adsorption–desorption cycle was conducted three times using the same nanoadsorbent. The desorption efficiency (E_D%) was determined according to the below formula:[38]

$$E_D\% = \frac{\text{quantity of desorbed uranium}}{\text{quantity of adsorbed uranium}} \times 100 \quad (13)$$

3. Results and discussions

3.1. Fe_3O_4@Cyanex-923 nanoadsorbent characterization

The size distribution and average particle size of Fe_3O_4@Cyanex-923 nanoadsorbent were determined by DLS analysis as displayed in Fig. 1(a). From the DLS graph, it can be noticed that Fe_3O_4@Cyanex-923 nanoparticles have a size distribution range of 15–95 nm with a mean particle size of 44.6 nm, as calculated by a Gaussian fit. The calculated polydispersity index (PI) of Fe_3O_4@Cyanex-923 nanoparticles is 0.199, which indicate a high homogeneity in the particles population.

TEM analysis was conducted to further investigate the particles size, structure, and surface morphology of Fe_3O_4@Cyanex-923. As is indicated from Fig. 1(b), Fe_3O_4@Cyanex-923 nanoparticles have a quasi-spherical structure of an average diameter of ~34.4 nm. The observed partial agglomeration in Fig. 1(b) could be due to the drying process and the tendency of the nanoparticles to aggregate that result from their large surface-to-volume ratio.[39] As can be noted, the average diameter observed by TEM measurement is relatively smaller than that obtained by DLS analysis. This is due to the fact that DLS calculates the particles diameter in liquid media, thus the hydrodynamic size measurements are usually greater than the actual nanoparticles size. This originates from the presence of extra solvent layers associated with the nanoparticles surface.[40] The surface morphology of Fe_3O_4@Cyanex-923 nanoadsorbent was further observed by SEM. The micrograph of Fe_3O_4@Cyanex-923, Fig. 1(c), shows nearly homogeneous grains with a smooth surface where most of the nanoparticles are quasi-spherical in shape.

The functional groups of Fe_3O_4@Cyanex-923 were identified by FTIR spectroscopy as shown in Fig. 2(a). The signals at 454 cm^{-1} and 588 cm^{-1} correspond to the characteristic Fe–O vibrations of the Fe_3O_4 core.[41] The signals at 1150 cm^{-1}, 1289 cm^{-1}, and 1460 cm^{-1} arise from P=O, O–P–O, and P–C stretching vibrations, respectively.[42] The signals at 1378 cm^{-1} and 2954 cm^{-1} represent the –CH_3 symmetric and dissymmetric stretching frequency, whereas the signals at 2854 cm^{-1} and 2924 cm^{-1} represent –CH_2 symmetric and dissymmetric stretching vibrations, respectively.[43] These results indicate that Cyanex-923 was successfully coated onto the Fe_3O_4 surface. The appearance of a broad peak around 3400 cm^{-1} could result from the water molecules adsorbed from the atmospheric moisture.

To investigate the thermal stability and quantify the surface coating of the Fe_3O_4 nanoparticles, TGA was performed and represented in Fig. 2(b). The TGA curve of Fe_3O_4@Cyanex-923 shows two-step degradation with a total mass loss of 35.5%,

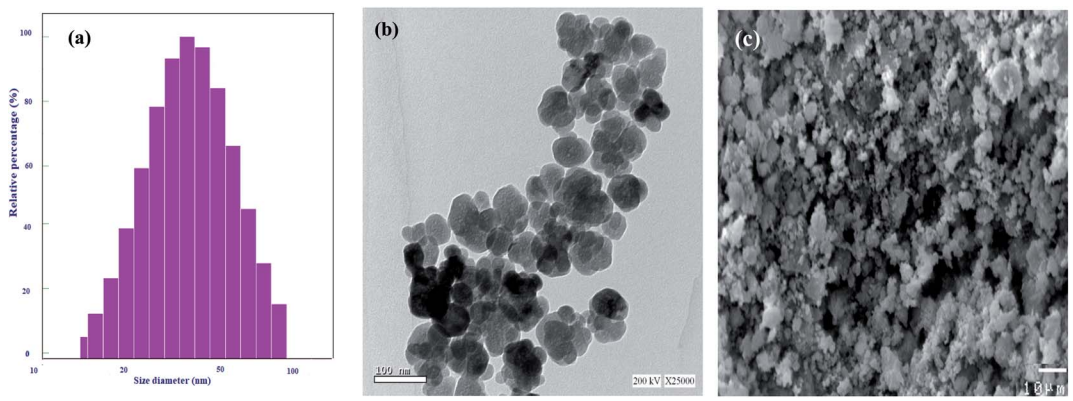

Fig. 1 (a) DLS, (b) HR-TEM, and (c) SEM micrographs of Fe_3O_4@Cyanex-923 nanoadsorbent.

which indicates that the magnetic content of Fe_3O_4@Cyanex-923 could be up to 64.5%. Fig. 2(b) reveals an initial 2.5% weight loss observed in the temperature range 88–180 °C which could be attributed to the loss of the adsorbed water. This is followed by a second 33% weight loss starts from 180 to 386 °C which is attributed to the decomposition of Cyanex-923 molecules onto the surface of Fe_3O_4 nanoparticles. No mass loss appears at $T >$ 400 °C, as the Fe_3O_4 residue is stable beyond 400 °C. TGA results confirm the successful coating of Cyanex-923 on Fe_3O_4 surface, since the TGA of bare Fe_3O_4 nanoparticle shows only 6% weight loss at 160 °C due to dehydration.[44]

Magnetization is a promising feature of Fe_3O_4-based adsorbents that allows for their facile separation from the treated solution. Thus, the magnetic properties of Fe_3O_4@Cyanex-923 were examined and the magnetic hysteresis loop was represented in Fig. 2(c). The nonlinear variation in magnetization as a function of the magnetic field (S shape) reveals that Fe_3O_4@Cyanex-923 nanoparticles are constituted by a single magnetic domain with negligible coercivity or remanence. This indicates the superparamagnetic character of Fe_3O_4@Cyanex-923. The relatively high value of the saturation magnetization (M_s) of Fe_3O_4@Cyanex-923 nanoadsorbent (64.5 emu g^{-1}) is good enough to enable its easy separation and recovery from the aqueous solutions by the conventional magnets.[45] Compared to bare Fe_3O_4 nanoparticles (M_s ~72 emu g^{-1}),[35] Fe_3O_4@Cyanex-923 shows a relatively lower M_s value. This is caused by the decrease of Fe_3O_4 fraction after Cyanex-923 coating and the surface spin effect on Fe_3O_4 nanoparticles that subsequently decrease the M_s value.[41]

3.2. pH effect on the adsorption performance of Fe_3O_4@Cyanex-923

Typically, the adsorbent performance is affected by the solution pH, as it affects the ionization degree of the adsorbent binding sites as well as the adsorbate solubility and speciation. Accordingly, the pH effect on the adsorption capacity of the prepared magnetic nanoadsorbent was investigated to determine the usable working range. Fig. 3(a) shows that the adsorption capacity of Fe_3O_4@Cyanex-923 increases with the pH increase to reach its utmost value at pH ~5 and then levels off. This behavior is similar to that reported for silica coated with alkylphosphine oxides,[32] as higher uranium(VI) adsorption was attained at pH 5. At low pH values, the predominant uranium species is UO_2^{2+} which competes with the abundant H^+ and H_3O^+ ions for the binding sites on the Fe_3O_4@Cyanex-923 surface,[46] and consequently the adsorption is unfavorable at low pH. Additionally, the pH affects the entire surface charge of Fe_3O_4@Cyanex-923 and the protonation of oxygen atoms in the P═O group at acidic media negatively affects the uranium(VI) adsorption due to the strong electrostatic repulsion. By increasing the pH, the surface becomes less positively charged and a greater number of binding sites becomes available for the adsorption of uranium ions. Additionally, the decrease of H^+ and H_3O^+ ions with the pH increase is favorable for uranium binding. Under weak acid conditions other positively charged uranium species dominate including $UO_2(OH)^+$, $(UO_2)_2(OH)_2^{2+}$ and $(UO_2)_3(OH)_5^+$ that could facilitate the electrostatic interaction with the Fe_3O_4@Cyanex-923 surface.[47] The observed decline in the adsorption efficiency over pH 5 results from the uranium hydrolysis and formation of precipitate ($UO_3 \cdot 2H_2O$)

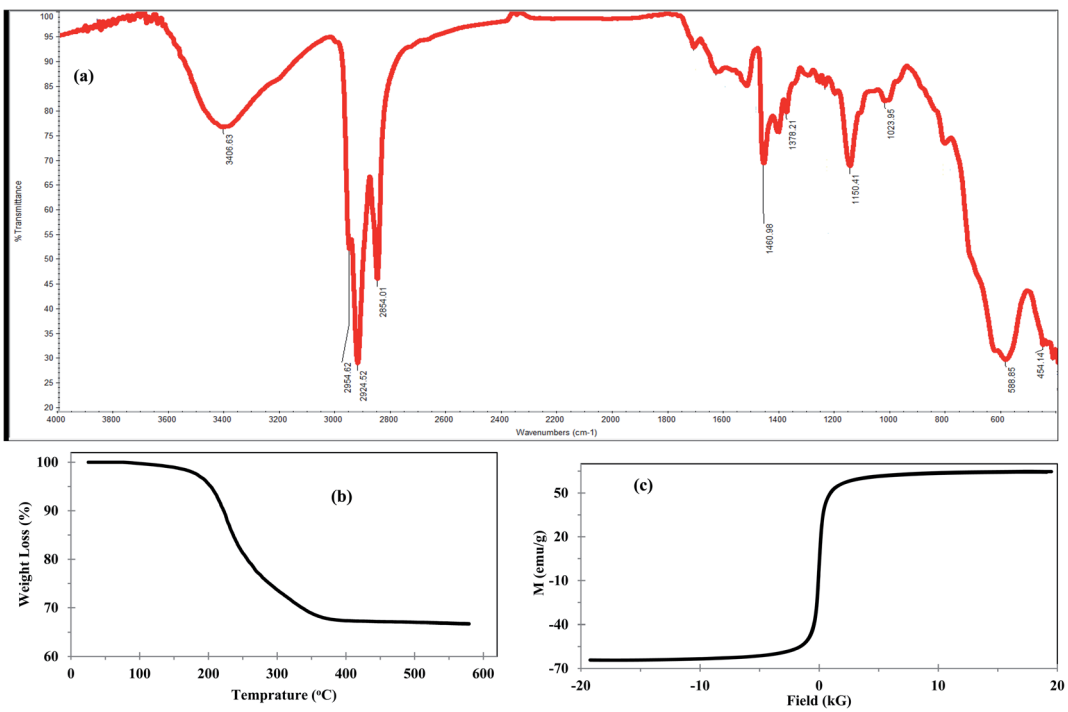

Fig. 2 (a) FTIR spectrum, (b) TGA curve, and (c) magnetization curve of Fe_3O_4@Cyanex-923 nanoadsorbent.

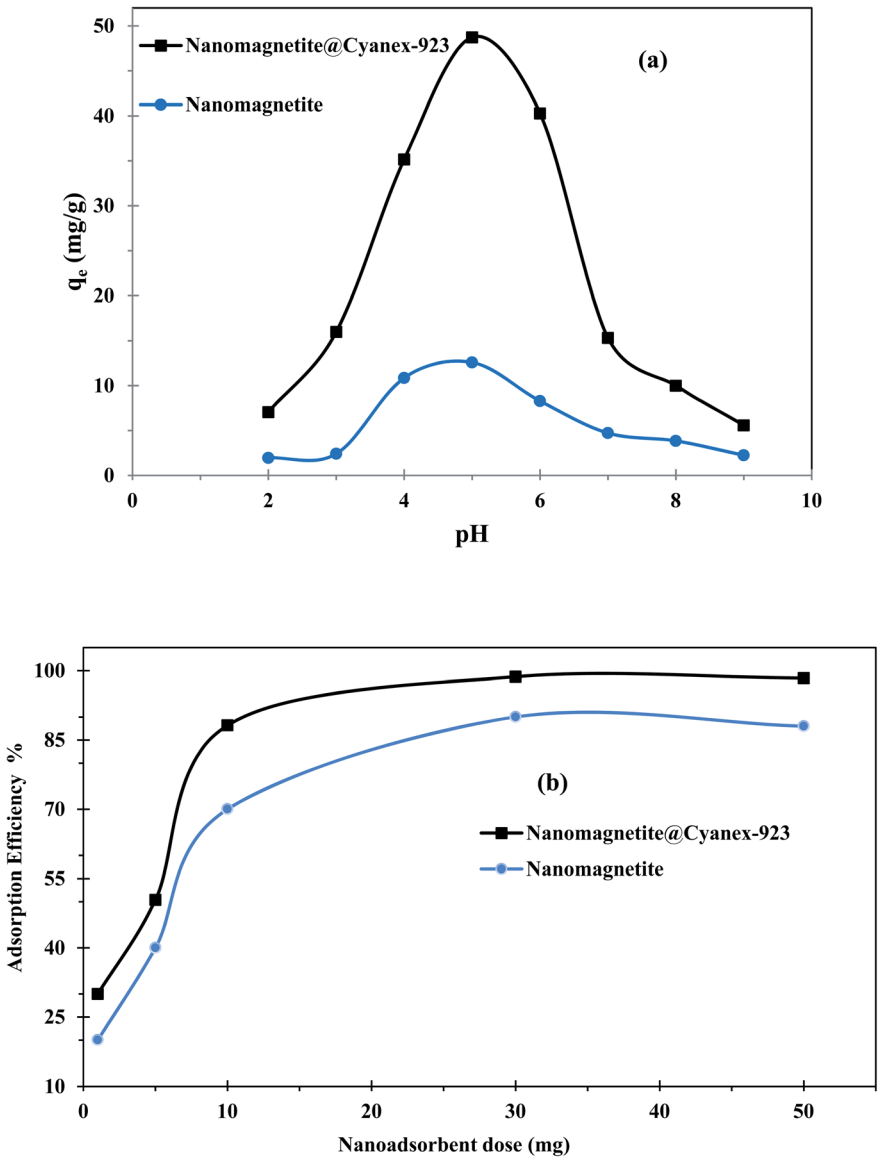

Fig. 3 Effect of (a) pH and (b) sorbent dose on uranium adsorption.

starting at pH ~5.5, thus decreases the overall uranium(VI) concentration.[28] As the pH moves beyond neutral, anionic uranium species such as $UO_2(OH)_3^-$, $(UO_2(OH)_4)^{2-}$, $(UO_2)_3(OH)_8^{2-}$, and $(UO_2(OH)_5)^{3-}$ dominate and their electrostatic repulsive interactions with the negatively charged surface of Fe_3O_4@Cyanex-923 cause a sharp decrease in the adsorption capacity.

The results of uranium adsorption on the bare magnetite nanoparticles demonstrate that the adsorption efficiency is dependent on the solution pH as shown in Fig. 3(a). This can be attributed to the influence of the medium acidity on the functional groups at the Fe_3O_4 surface. Fe_3O_4 is an amphoteric solid that is capable to develop charges *via* the protonation and deprotonation of –FeOH sites on its surface with the pH change as follows.[47,48]

$$–FeOH + H^+ \Leftrightarrow –FeOH_2^+ \quad (14)$$

$$–FeOH_2^+ – H_2O \Leftrightarrow –Fe^+ \quad (15)$$

$$–FeOH_2^+ \Leftrightarrow –FeOH + H^+ \quad (16)$$

$$–FeOH \Leftrightarrow –FeO^- + H^+ \quad (17)$$

At low pHs, the H^+ ions exist in excess that causes the protonation of the –OH on the surface of Fe_3O_4 and accordingly the $–FeOH_2^+$ content increase, resulting in electrostatic repulsion with positively charged uranium(VI) ions.[47] With the pH increase, more adsorption sites on the Fe_3O_4 surface turn into the more reactive deprotonated and negatively charged forms, thereby leading to a higher uptake of uranium(VI) ions.[48] With further pH value increase, the anionic uranium species are formed that do not tend to bind to the negatively charged Fe_3O_4 surface.

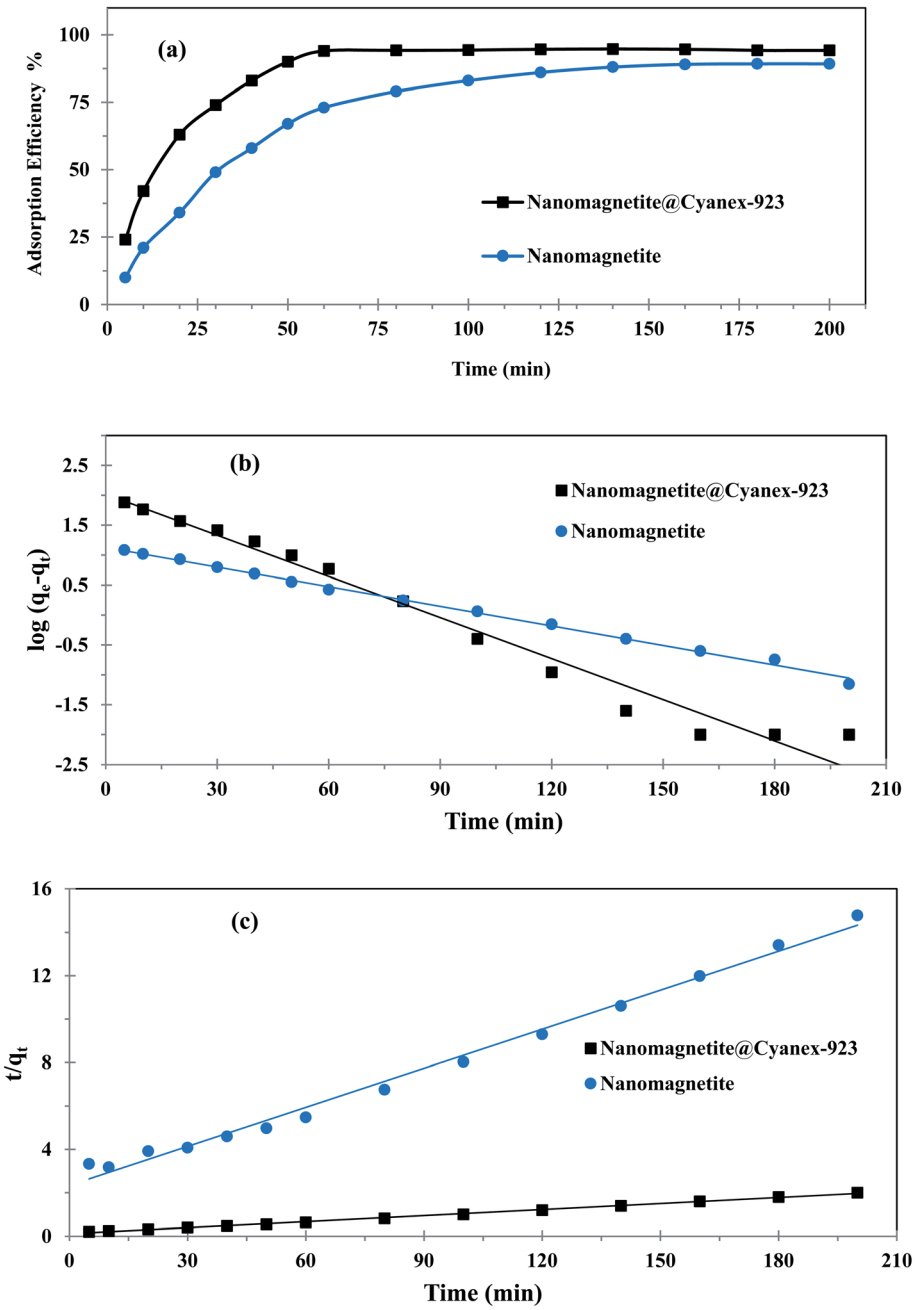

Fig. 4 (a) Effect of contact time on uranium adsorption, (b) pseudo-1st-order, and (c) pseudo-2nd-order kinetics models fitting curves.

3.3. Dosage effect on the adsorption performance of Fe_3O_4@Cyanex-923

To maximize the interaction between uranium(VI) ions and the active sites of magnetic nanoadsorbent, the nanoadsorbent mass was varied from 1 to 50 mg while maintaining all other factors fixed. The corresponding adsorption efficiency was determined and presented in Fig. 3(b). As can be noticed the adsorption efficiency of Fe_3O_4@Cyanex-923 and bare Fe_3O_4 nanoparticles first increases with the adsorbent dose increment reaching its maximum at 30 mg. Further increase of nano-adsorbent dose doesn't cause a significant increase of the adsorption efficiency. Initially, the higher nanoadsorbent dose provides a larger surface area and more adsorption sites for uranium(VI) ions till a plateau is reached. At this point, the uranium(VI) quantity adsorbed per nanoadsorbent unit weight keeps constant where more unoccupied active sites would no longer contribute to the adsorption process.[49] Considering factors of adsorption efficiency and economic cost, 30 mg was considered as the optimal dose in next experiments.

3.4. Adsorption kinetics

When optimizing the adsorption systems design, particularly for industrial applications, it is of paramount importance to explore the adsorption kinetics. Thus, the adsorption efficiency

Table 1 Kinetic parameters of pseudo-1st-order and pseudo-2nd-order models

		Pseudo first-order				Pseudo second-order				
Adsorbent	$q_{e,exp}$ (mg g^{-1})	$q_{e,cal}$ (mg g^{-1})	k_1 (min^{-1})	R^2	χ^2	$q_{e,cal}$ (mg g^{-1})	$k_2 \times 10^{-3}$ (g mg^{-1} min^{-1})	R^2	χ^2	h (mg g^{-1} min^{-1})
Fe_3O_4@Cyanex-923	99.862	127.938	0.052	0.974	8.453	108.695	0.719	0.997	0.949	8.503
Fe_3O_4 nanoparticles	13.601	13.365	0.025	0.996	0.063	16.666	1.534	0.981	0.691	0.427

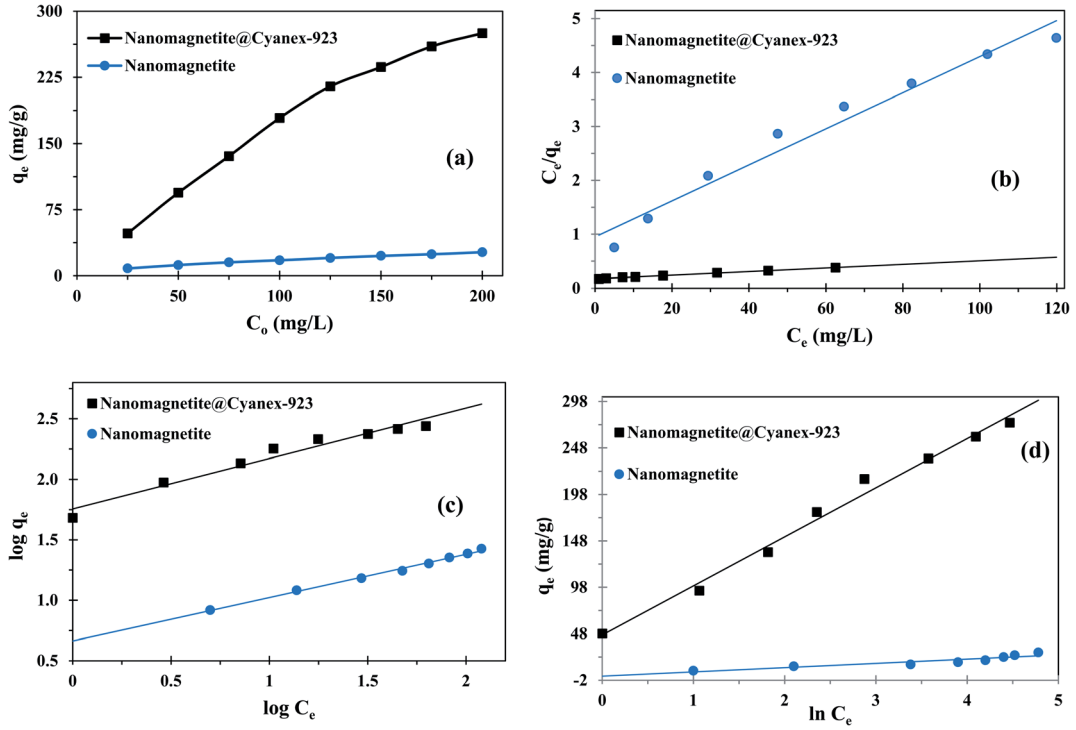

Fig. 5 (a) Effect of initial uranium concentration on the adsorption capacity, (b) Langmuir, (c) Freundlich, and (d) Temkin isotherms fitting curves.

was monitored over time to examine how the contact time affects the adsorption process. Fig. 4(a) reveals that the adsorption efficiency of uranium(VI) first increases sharply with contact time by virtue of the presence of availably abundant adsorption sites at the magnetic nanoadsorbent surface. This behavior indicates the increase of driving force for mass transfer and thus further uranium(VI) ions reach the surface of the magnetic nanoadsorbent within a short time. Afterward, the adsorption efficiency continues to increase at a slower rate, and eventually reaches equilibrium and then remains steady for the rest of the time as the vacant binding sites on the magnetic nanoadsorbent surface are almost consumed.

As can be noticed from Fig. 4(a), Fe_3O_4@Cyanex-923 shows a faster equilibrium time (60 min) compared to bare Fe_3O_4 (180 min). The fast equilibrium state achieved by Fe_3O_4@Cyanex-923 is caused by the strong chelation of uranium ions with phosphine oxide functional groups. Additionally, the adsorbent nanoscale structure gives a share in the fast diffusion. According to the kinetic results, Fe_3O_4@Cyanex-923 could have real-world applications potential for uranium removal from sizable amounts of water.

To describe the rate-controlling step of uranium(VI) adsorption on the prepared nanoadsorbent, the pseudo-1st-order and pseudo-2nd-order models were employed and the corresponding fitting curves were illustrated in Fig. 4(b) and (c), respectively. The related kinetic parameters calculated from these models were summarized in Table 1. According to the results, the pseudo-2nd-order model reveals a better regression analysis for Fe_3O_4@Cyanex-923 experimental data ($R^2 = 0.997$), thus the uranium(VI) adsorption process on Fe_3O_4@Cyanex-923 obeys the pseudo-2nd-order kinetic equation. Additionally, the adsorption capacity obtained from the pseudo-2nd-order model (108.695 mg g^{-1}) is nearer to the experimental value (99.862 mg g^{-1}) compared to that obtained from the pseudo-1st-order model (127.938 mg g^{-1}). The lower χ^2 value obtained for the pseudo-2nd-order model further validates that this model is ideal for explaining the uranium(VI) adsorption behavior on Fe_3O_4@Cyanex-923. These results indicate that the dominant interaction of uranium(VI) ions with the active sites on the

Table 2 Isotherm parameters of Langmuir, Freundlich, and Temkin models

	Fitting parameters at 25 °C, pH 5	
Adsorption isotherm	Fe_3O_4@Cyanex-923	Fe_3O_4 nanoparticles
Langmuir	$R^2 = 0.997$ $q_{max} = 429.185$ (mg g^{-1}) $K_L = 0.099$ (L mg^{-1})	$R^2 = 0.927$ $q_{max} = 29.850$ (mg g^{-1}) $K_L = 0.041$ (L mg^{-1})
Freundlich	$R^2 = 0.958$ $K_F = 57.003$ (mg g^{-1}) $n = 2.402$ (L mg^{-1}) $1/n = 0.416$	$R^2 = 0.994$ $K_F = 4.611$ (mg g^{-1}) $n = 2.792$ (L mg^{-1}) $1/n = 0.358$
Temkin	$R^2 = 0.988$ $A_T = 2.559$ (L g^{-1}) $B = 52.849$ (J mol^{-1})	$R^2 = 0.805$ $A_T = 1.496$ (L g^{-1}) $B = 4.590$ (J mol^{-1})

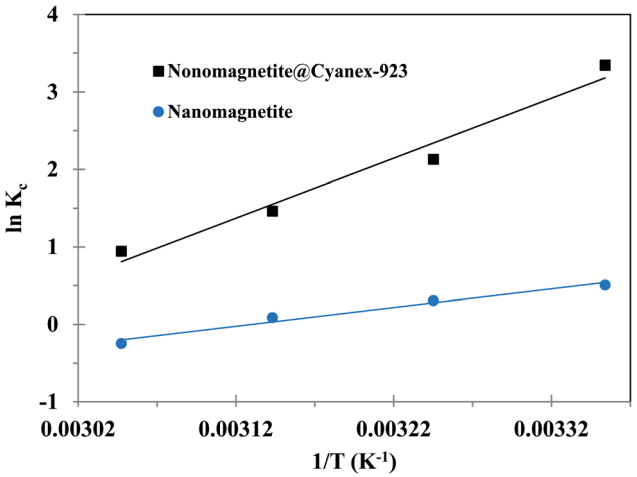

Fig. 6 van't Hoff plot for uranium(VI) adsorption.

Fe_3O_4@Cyanex-923 surface is a chemical one,[50] where the adsorption rate is governed by chemical chelation *via* sharing or exchanging electrons at the solid/solution interface.

Contradictory, data in Table 1 points out that adsorption kinetics of uranium(VI) on bare Fe_3O_4 nanoparticles could be better explained by the pseudo-1st-order model. It can be noted that q_e value of uranium adsorption on bare Fe_3O_4 calculated by the pseudo-1st-order model is more consistent with the experimental value. Moreover, pseudo-1st-order model reveals a better fitting with higher correlation coefficient (R^2) than the pseudo-2nd-order.

3.5. Adsorption isotherms

Fig. 5(a) displays how the adsorption capacity of Fe_3O_4@Cyanex-923 and bare Fe_3O_4 is affected by the variation of uranium(VI) initial concentration. It can be noticed that, at a constant adsorbent dose, the adsorption capacity increases upon increasing the uranium concentration in the solution. At higher initial concentrations, the driving force needed to defeat the ions mass-transfer resistance increase, resulting in a better interaction between uranium(VI) ions and the active sites of the nanoadsorbent,[51] which eventually leads to higher uranium(VI) uptake for a given magnetic nanoadsorbent mass.

To understand the adsorption mechanism and predict the maximum adsorption capacity; the isotherm studies were carried out using Langmuir, Freundlich, and Temkin equations; and the obtained results were represented in Fig. 5(b), (c), and (d), respectively. The corresponding fitting parameters were tabulated in Table 2.

Langmuir isotherm assumes single-layered chemisorption onto the adsorbent surface that has similar binding positions and equivalent adsorption energies with no steric hindrance. In contrast, Freundlich isotherm assumes a multiple-layered adsorption at heterogonous surfaces where there are interactions between adsorbed molecules.[28] Fitting the experimental results of uranium adsorption on Fe_3O_4@Cyanex-923 to the Langmuir and Freundlich models gave R^2 values of 0.997 and 0.958, respectively. It can be noted that Freundlich model showed a lower R^2 value compared to the Langmuir model, suggesting that Langmuir model is better fitted with the Fe_3O_4@Cyanex-923 adsorption data and a homogenous single-layered adsorption dominates the process. On the contrary, the fitting coefficient for bare magnetite nanoparticles is greater for Freundlich isotherm than Langmuir isotherm, suggesting the suitability of Freundlich model to the adsorption data of brae Fe_3O_4 and the existence of heterogeneous adsorption sites.

The maximum single-layer adsorption capacity of uranium(VI) on Fe_3O_4@Cyanex-923 and bare Fe_3O_4 nanoparticles was calculated by Langmuir isotherm as 429.185 and 29.850 mg g^{-1}, respectively. The results clearly indicate the higher affinity of Fe_3O_4@Cyanex-923 towards uranium(VI) ions, hence it could be considered as a promising material for uranium(VI) adsorption from aqueous solutions. The R_L values were less than unity for both Fe_3O_4@Cyanex-923 and bare Fe_3O_4 (0.048–0.993), indicating that the adsorption process is suitable for both magnetic nanoadsorbents.

The higher value of Freundlich constant for Fe_3O_4@Cyanex-923 ($K_F = 57.003$ L g^{-1}) compared to bare Fe_3O_4 ($K_F = 4.611$ L g^{-1}) indicates the higher adsorption capacity of Fe_3O_4@Cyanex-923 that results from the strong affinity of Fe_3O_4@Cyanex-923 to uranium(VI) ions.[52] The n values of Fe_3O_4@Cyanex-923 and bare Fe_3O_4 lies between 1 and 10, indicating a favorable adsorption process. The n value is slightly higher for bare Fe_3O_4

Table 3 Thermodynamic parameters for uranium(VI) ions adsorption

	ΔH° (kJ mol^{-1})	ΔS° (kJ mol^{-1} K^{-1})	Temp. (K)	ΔG° (kJ mol^{-1})
Fe_3O_4@Cyanex-923	−64.381	0.189	298	−8.296
			308	−5.457
			318	−3.870
			328	−2.576
Fe_3O_4 nanoparticles	−20.061	0.147	298	−1.256
			308	−0.782
			318	−0.233
			328	−0.075

nanoparticles, denoting the increased heterogeneity of the adsorption.[53]

Temkin isotherm is another model that assumes the dependence of the adsorption free energy on the adsorbent surface coverage, as the adsorption heat linearly decreases because of the adsorbent–adsorbate interactions. The plot of Temkin isotherm fitted quite well to the experimental data obtained for Fe_3O_4@Cyanex-923 (R^2 = 0.988) which further elucidates the chemisorption adsorption process.[36] The poor-fit of the uranium(VI) adsorption data on bare Fe_3O_4 nanoparticles to Temkin model indicates the unsuitability of this model to describe the uranium(VI) interaction with bare Fe_3O_4. The B value calculated for Fe_3O_4@Cyanex-923 is 52.849 J mol^{-1} which confirmed that the uranium(VI) adsorption process onto Fe_3O_4@Cyanex-923 is a chemisorption one.[54] The positive value of B made it clear that the adsorption is exothermic for Fe_3O_4@Cyanex-923 supporting the obtained thermodynamics results.[55]

3.6. Adsorption thermodynamics

To foresee the effect of the uranium(VI) adsorption on the solution temprature, adsorption experiments were carried out under a temperature range of 298 to 328 K. The results revealed that the adsorption capacity of Fe_3O_4@Cyanex-923 and bare Fe_3O_4 nanoparticles gradually decreases upon increasing the temperature; signifying the exothermic nature of the adsorption process. Such behavior is attributed to the equilibrium shift toward desorption accompanied by weaker uranium–adsorbent interactions resulted from the increased molecular mobility and lower chemical affinity when the temperature is raised.

Generally, the thermodynamic parameters offer in-depth data concerning the spontaneity and feasibility of the adsorption process. Thus, the van't Hoff plot, Fig. 6, was used to calculate the thermodynamic parameters of uranium adsorption on Fe_3O_4@Cyanex-923 and bare Fe_3O_4 nanoparticles and the data was listed in Table 3. It is clear that low temperature is favorable for uranium adsorption on Fe_3O_4@Cyanex-923 and bare Fe_3O_4, as interpreted from the decrease of ΔG° values with temperature increasing. It is noticed that the K_c values decrease with the temperature rise, signifying an exothermic process.[54] The negative ΔG° values indicate the spontaneity and feasibility of uranium adsorption on Fe_3O_4@Cyanex-923 and bare Fe_3O_4 under the studied temperatures.[54] The negative ΔH° values further affirm the exothermic character of the adsorption process. ΔS° positive values suggest the increase of randomness at the solid/solution interface resulting from the decrease in molecular orderliness during the adsorption process.[28]

3.7. Desorption and reusability

Generally, the adsorbent regeneration and recycling are desirable to attain a feasible and economic adsorption process. Thus, to investigate the reusability of the magnetic nano-adsorbent, Fe_3O_4@Cyanex-923 and bare Fe_3O_4 were subjected to repetitive adsorption and desorption experiments in three consecutive cycles. Both nitric acid and sodium carbonate were tested for their effectiveness as eluent reagents. The results illustrated in Fig. 7 clearly show that uranium ions could be desorbed from Fe_3O_4@Cyanex-923 and bare Fe_3O_4 by 0.01 mol L^{-1} HNO_3 and 0.5 mol L^{-1} Na_2CO_3 solution. A desorption efficiency of 95–90% and 98–95.5% was obtained over 3 cycles by HNO_3 and Na_2CO_3, respectively, for Fe_3O_4@Cyanex-923. On the other hand, a lower desorption efficiency was observed for bare Fe_3O_4 nanoparticles (88–71 and 95–85% for HNO_3 and Na_2CO_3, respectively).

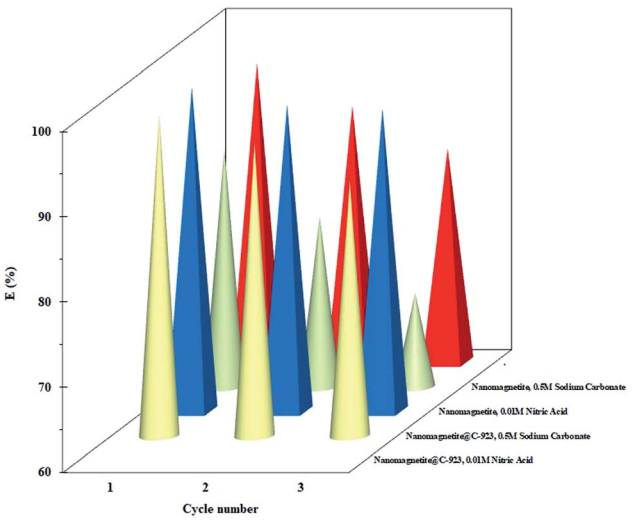

Fig. 7 Effect of desorption agents on the desorption efficiency of U(VI) from Fe_3O_4@Cyanex-923 and bare Fe_3O_4 for three continues cycles.

Table 4 Comparison of uranium adsorption performance of Fe_3O_4@Cyanex-923 with other magnetic adsorbents

Adsorbent	pH	Temperature °C	q_{max} (mg g^{-1})	Time	Ref.
Fe_3O_4 nanoparticles	7.0	25	5.5	4–6 h	22
Fe_3O_4@GO	5.5	25	69.5	4 h	23
Amidoxime modified Fe_3O_4@SiO_2	5.0	25	105	24 h	24
PAAM-FeS/Fe_3O_4	5.0	20	311	1 h	25
Magnetic oxine	7	25	125	4 h	26
Fe_3O_4@C@Ni-Al LDH	6	25	227	3 h	27
Fe_3O_4@MS	5.5	25	242.5	5 h	28
Fe_3O_4@TiO_2	6.0	25	118.8	4 h	56
Fe_3O_4@SiO_2	6.0	25	52		57
Fe_3O_4@C-KO	6.0	25	38.7	2 h	58
Fe_3O_4@C@ASA	4	25	46.2	4 h	59
Fe_3O_4@PAM	5	20	220.9	NA	60
Fe_3O_4@phosphoramide	6	25	95.2	1.25	61
Magnetic schiff base	6	25	94.3	6 h	62
Fe_3O_4@Cyanex-923	5	25	429.1	1 h	This work

It can be indicated from the results that higher recovery of U(VI) species from the loaded Fe_3O_4@Cyanex-923 and bare Fe_3O_4 could be obtained using 0.5 mol L^{-1} Na_2CO_3 solution.

3.8. Comparison of Fe_3O_4@Cyanex-923 performance with other magnetic adsorbents

The literature reveals that a number of reagents were immobilized onto Fe_3O_4 core and used for uranium removal from different matrices. Table 4 shows the adsorption behavior of Fe_3O_4@Cyanex-923 towards uranium compared to the previously reported magnetic adsorbents[22–28,56–62] in terms of adsorption capacity, experimental conditions, and equilibrium time. It can be noted that the q_{max} value of Fe_3O_4@Cyanex-923 is excellent compared to the listed magnetic adsorbents. The high adsorption capacity of Fe_3O_4@Cyanex-923 mainly results from the phosphine oxide groups distributed on the surface of Fe_3O_4 nanoparticles, thus uranium ions could have access to the adsorption sites easily during the adsorption process. It can be observed that Fe_3O_4@Cyanex-923 reveals the advantage of lower equilibration time which is essential in large volume samples and at an industrial scale. Table 4 suggests that Fe_3O_4@Cyanex-923 has a great potential as a uranium(VI) adsorbent.

4. Conclusions

The results of this work demonstrated that Fe_3O_4@Cyanex-923 nanoadsorbent is especially conceived for efficient removal of uranium(VI) ions from aqueous solutions. The optimal conditions for uranium(VI) adsorption were as follows: adsorption temperature = 25 °C, adsorption time = 60 min, Fe_3O_4@Cyanex-923 weight = 30 mg, and solution pH value = 5. Treating the experimental data with various kinetics and isotherms models indicated that the adsorption of uranium on Fe_3O_4@Cyanex-923 is a monolayer chemisorption process that is well-correlated to pseudo-2nd-order and Langmuir equations. Fe_3O_4@Cyanex-923 can be as easily separated by applying an external magnetic field and after three cycles the adsorption and desorption capacities of the magnetic adsorbent were still high. Fe_3O_4@Cyanex-923 adsorption capacity for uranium(VI) almost matched or exceeded that of reported magnetic adsorbents in the literature. Compared to bare Fe_3O_4 nanoparticles, the adsorption capacity and stability of Fe_3O_4@Cyanex-923 were greatly enhanced upon modification.

Conflicts of interest

There are no conflicts to declare.

Acknowledgements

The author would like to express her great thanks to Prof. J. A. Doud, Egyptian atomic energy authority, for her kind support.

References

1 G. Fadillah, S. P. Yudha, S. Sagadevan, I. Fatimah and O. Muraza, *Open Chem.*, 2020, **18**, 1148.
2 D. Mehta, S. Mazumdar and S. K. Singh, *J. Water Process. Eng.*, 2015, **7**, 244.
3 N. Gupta, P. Pant, C. Gupta, P. Goel, A. Jain, S. Anand and A. Pundir, *Mater. Res. Innovations*, 2018, **22**, 434.
4 M. Yu, L. Wang, L. Hu, Y. Li, D. Luo and S. Me, *Trends Anal. Chem.*, 2019, **119**, 115611.
5 Q. Zhou, J. Li, M. Wang and D. Zhao, *Crit. Rev. Environ. Sci. Technol.*, 2016, **46**, 783.
6 S. M. Husnain, W. Um, W. Lee and Y. S. Chang, *RSC Adv.*, 2018, **8**, 2521.
7 J. Wallyn, N. Anton and T. F. Vandamme, *Pharmaceutics*, 2019, **11**, 601.
8 G. A. Bird, Uranium in the environment: Behavior and toxicity, in *Encyclopedia of isustainability science and technology*, ed. R. A. Meyers, Springer, New York, NY, 2012.
9 D. Brugge and V. Buchner, *Rev. Environ. Health*, 2011, **26**, 231.
10 B. Hu, H. Wang, R. Liu and M. Qiu, *Chemosphere*, 2021, **274**, 129743.

11 H. Guo, P. Mei, J. Xiao, X. Huang, A. Ishag and Y. Sun, *Chemosphere*, 2021, **278**, 130411.
12 R. Liu, H. Wang, L. Han, B. Hu and M. Qiu, *Environ. Sci. Pollut. Res. Int.*, 2021, **28**, 55176–55185.
13 A. Ishag and Y. Sun, *Ind. Eng. Chem. Res.*, 2021, **60**, 8007.
14 M. Qiu, Z. Liu, S. Wang and B. Hu, *Environ. Res.*, 2021, **196**, 110349.
15 X. Zhong, Z. Lu, W. Liang, X. Guo and B. Hu, *Environ. Sci.: Nano*, 2020, **7**, 3303.
16 N. Zhang, A. Ishag, Y. Li, H. Wang, H. Guo, P. Mei, Q. Meng and Y. Sun, *J. Cleaner Prod.*, 2020, **277**, 123360.
17 F. Zahran, H. H. El-Maghrabi, G. Hussein and S. M. Abdelmaged, *Environ. Nanotechnol. Monit. Manag.*, 2019, **11**, 100205.
18 J. Wu, K. Tian and J. Wang, *Prog. Nucl. Energy*, 2018, **106**, 79.
19 L. Tan, Y. Wang, Q. Liu, J. Wang, X. Jing, L. Liu, J. Liu and D. Song, *Chem. Eng. J.*, 2015, **259**, 752.
20 S. Tsarev, R. N. Collins, E. S. Ilton, A. Fahy and T. D. Waite, *Environ. Sci.: Nano*, 2017, **4**, 1304.
21 T. Zhang, J. Chen, H. Xiong, Z. Yuan, Y. Zhu and B. Hu, *Chemosphere*, 2021, **283**, 131241.
22 R. A. Crane, M. Dickinson, I. C. Popescu and T. B. Scott, *Water Res.*, 2011, **45**, 2931.
23 P. Zong, S. Wang, Y. Zhao, H. Wang, H. Pan and C. He, *Chem. Eng. J.*, 2013, **220**, 45.
24 Y. Zhao, J. Li, L. Zhao, S. Zhang, Y. Huang, X. Wu and X. Wang, *Chem. Eng. J.*, 2014, **235**, 275.
25 D. Shao, X. Wang, J. Li, Y. Huang, X. Ren, G. Hou and X. Wang, *Environ. Sci.: Water Res. Technol.*, 2015, **1**, 169.
26 L. Tan, J. Wang, Q. Liu, Y. Sun, H. Zhang, Y. Wang, X. Jing, J. Liu and D. Song, *Colloids Surf., A*, 2015, **466**, 85.
27 X. Zhang, J. Wang, R. Li, Q. Dai, R. Gao, Q. Liu and M. Zhang, *Ind. Eng. Chem. Res.*, 2013, **52**, 10152.
28 M. Zeng, Y. Huang, S. Zhang, S. Qin, J. Li and J. Xu, *RSC Adv.*, 2014, **4**, 5021.
29 W. Zhang, G. Ye and J. Chen, *J. Mater. Chem. A*, 2013, **1**, 12706.
30 W. Zhang, A. Bu, Q. Ji, L. Min, S. Zhao, Y. Wang and J. Chen, *ACS Appl. Mater. Interfaces*, 2019, **11**, 33931.
31 W. Zhang, G. Ye and J. Chen, *Sep. Sci. Technol.*, 2013, **48**, 263.
32 W. Zhang, G. Ye and J. Chen, *RSC Adv.*, 2016, **6**, 1210.
33 X. Yuan, Y. Cai, L. Chen, S. Lu, X. Xiao, L. Yuan and W. Feng, *Sep. Purif. Technol.*, 2020, **230**, 115843.
34 S. K. Sahu, M. L. P. Reddy, T. R. Ramamohan and V. Chakravortty, *Radiochim. Acta*, 2000, **88**, 33.
35 C. Basualto, J. Gaete, L. Molina, F. Valenzuela, C. Yañez and J. F. Marco, *Sci. Technol. Adv. Mater.*, 2015, **16**, 3.
36 N. Tang, C. G. Niu, X. T. Li, C. Liang, H. Guo, L. S. Lin, C. W. Zheng and G. M. Zeng, *Sci. Total Environ.*, 2018, **635**, 1331.
37 H. K. Boparai, M. Joseph and D. M. O'Carroll, *J. Hazard. Mater.*, 2011, **186**, 458.
38 M. Kumar, A. K. Singh and M. Sikandar, *Appl. Water Sci.*, 2018, **8**, 225.
39 D. Das, M. K. Sureshkumar, S. Koley, N. Mithal and C. G. S. Pillai, *J. Radioanal. Nucl. Chem.*, 2010, **285**, 447.
40 C. Das, S. Sen, T. Singh, T. Ghosh, S. S. Paul, T. W. Kim, S. Jeon, D. K. Mait, J. Im and G. Biswas, *Nanomaterials*, 2020, **10**, 1615.
41 Y. Wei, B. Han, X. Hu, Y. Lin, X. Wang and X. Deng, *Procedia Eng.*, 2012, **27**, 632.
42 S. Wei, J. Liu, S. Zhang, X. Chen, Q. Liu, L. Zhu, L. Guo and X. Li, *Hydrometallurgy*, 2016, **164**, 219.
43 D. C. Onwudiwe, M. Hrubaru and E. E. Ebenso, *J. Nanomater.*, 2015, **2015**, 143632.
44 H. Neelamegan, D. Yang, G. J. Lee, A. Sambandam, A. Sorrentino and J. J. Wu, *ACS Omega*, 2020, **5**, 7201.
45 D. D. Shao, C. L. Chen and X. K. Wang, *Chem. Eng. J.*, 2012, **185–186**, 144.
46 S. M. Husnain, H. J. Kim, W. Um, Y. Y. Chang and Y. S. Chang, *Ind. Eng. Chem. Res.*, 2017, **56**, 9821.
47 J. Zhang, S. Lin, M. Han, Q. Su, L. Xi and Z. Hui, *Water*, 2020, **12**, 446.
48 X. S. Wang, H. J. Lu, L. Zhu, F. Liu and J. J. Ren, *Adsorpt. Sci. Technol.*, 2010, **28**, 407.
49 E. S. Dragan, D. F. A. Loghin and A. I. Cocarta, *ACS Appl. Mater. Interfaces*, 2014, **6**, 16577.
50 L. Li, F. Wang, Y. Lv, J. Liu, D. Zhang and Z. Shao, *Appl. Clay Sci.*, 2018, **161**, 225.
51 J. Tao, J. Q. Xiong, C. L. Jiao, D. S. Zhang, H. Lin and Y. Y. Chen, *ACS Sustainable Chem. Eng.*, 2016, **4**, 60.
52 S. Rattanapan, J. Sirikram and P. Kongsune, *Procedia Eng.*, 2017, **138**, 949.
53 F. T. Kamga, *Appl. Water Sci.*, 2019, **9**, 1.
54 J. Wang, G. Liu, T. Lia and C. Zhou, *RSC Adv.*, 2015, **5**, 29859.
55 U. A. Edet and A. O. Ifelebuegu, *Processes*, 2020, **8**, 665.
56 L. Tan, X. Zhang, Q. Liu, X. Jing, J. Liu, D. Song, S. Hu, L. Liu and J. Wang, *Colloids Surf., A*, 2015, **469**, 279.
57 F. L. Fan, Z. Qin, J. Bai, W. D. Rong, F. Y. Fan, W. Tian, X. L. Wu, Y. Wang and L. Zhao, *J. Environ. Radioact.*, 2012, **106**, 40.
58 Q. Liu, W. T. Li, W. Zhao, L. C. Zhao, X. Y. Jing, J. Y. Liu, D. L. Song, H. S. Zhang, R. M. Li, L. H. Liu and J. Wang, *RSC Adv.*, 2016, **6**, 62179.
59 P. Li, J. Wang, X. Wang, B. He, D. Pan, J. Liang, F. Wang and Q. Fan, *J. Mol. Liq.*, 2018, **269**, 441.
60 W. C. Song, M. C. Liu, R. Hu, L. X. Tan and J. X. Li, *Chem. Eng. J.*, 2014, **246**, 268.
61 P. Singhal, B. G. Vats, A. Yadav and V. Pulhani, *J. Hazard. Mater.*, 2020, **384**, 121353.
62 X. Zhang, C. Jiao, J. Wang, Q. Liu, R. Li, P. Yang and M. Zhang, *Chem. Eng. J.*, 2012, **198–199**, 412.